Enhanced Triboelectric Nanogenerators and Triboelectric Nanosensor Using Chemically Modified TiO_2 Nanomaterials

Zong-Hong Lin,[†] Yannan Xie,[†] Ya Yang,[†] Sihong Wang,[†] Guang Zhu,[†] and Zhong Lin Wang[†,‡,*]

[†]School of Material Science and Engineering, Georgia Institute of Technology, Atlanta, Georgia 30332-0245, United States and [‡]Beijing Institute of Nanoenergy and Nanosystems, Chinese Academy of Sciences, China

ABSTRACT Mechanical energy harvesting based on triboelectric effect has been proven to be a simple, cost-effective, and robust method for electricity generation. In this study, we developed a rationally designed triboelectric nanogenerator (TENG) by utilizing the contact electrification between a polytetrafluoroethylene (PTFE) thin film and a layer of TiO_2 nanomaterial (nanowire and nanosheet) array. The as-developed TENG was systematically studied and demonstrated as a self-powered nanosensor toward catechin detection. The high sensitivity (detection limit of 5 μM) and selectivity are achieved through a strong interaction between Ti atoms of TiO_2 nanomaterial and enediol group of catechin. The output voltage and current density were increased by a factor of 5.0 and 2.9, respectively, when adsorbed with catechin of a saturated concentration, because of the charge transfer from catechin to TiO_2. This study demonstrates the possibility of improving the electrical output of TENG through chemical modification.

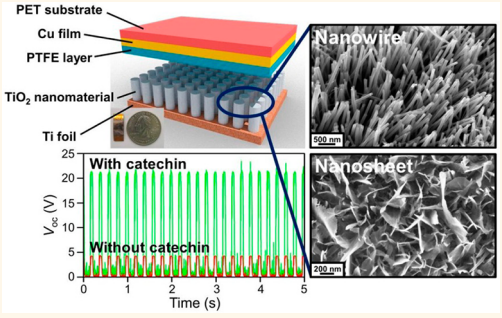

KEYWORDS: TiO_2 · catechin · nanosensor · chemical modification · triboelectric effect · charge transfer

In the past decades, increasing research efforts have been devoted to renewable energy owing to the largely increased energy consumption. Searching for renewable energy with reduced carbon emissions, secure long-term energy supply, and less dependence on fossil fuel is mandatory for the sustainable development of the world. Nanogenerators and solar cells, which are emerging new energy technologies that harvest renewable energy from mechanical vibration,[1,2] heat[3,4] and light[5,6] in the environment, are capable of fulfilling the above-mentioned features and have thus attracted global attention. Among different energy sources, mechanical vibration is the most promising candidate for the development of nanogenerators because the energy source is ubiquitous and accessible in our living environment. Since 2006, piezoelectric nanogenerators[7,8] have been developed to efficiently convert tiny-scale mechanical vibration into electricity. Until recently, another cost-effective, easy fabrication, and robust nanogenerator[9,10] has been created based on the triboelectric effect.

Triboelectric nanogenerator (TENG) harvests mechanical energy through a periodic contact and separation of two different materials.[11] Contact between two materials with different triboelectric polarity yields surface charge transfer. A periodic contact and separation of the oppositely charged surfaces can create a dipole layer and a potential drop, which drives the flow of electrons through an external load in responding to the mechanical vibration. TENG has been systematically studied as a power source that can drive instantaneous operation of light-emitting diodes (LEDs)[12] and charge a lithium ion battery as a regulated power module for powering a wireless sensor system and a commercial cell phone.[13] As for TENG, increasing the charge generation can be achieved by selecting materials with larger difference in the ability to attract and retain electrons,[14] changing the substrate morphology,[15] and enlarging the contact area of materials.[16,17]

* Address correspondence to zlwang@gatech.edu.

Received for review March 12, 2013 and accepted April 16, 2013.

Published online April 18, 2013
10.1021/nn401256w

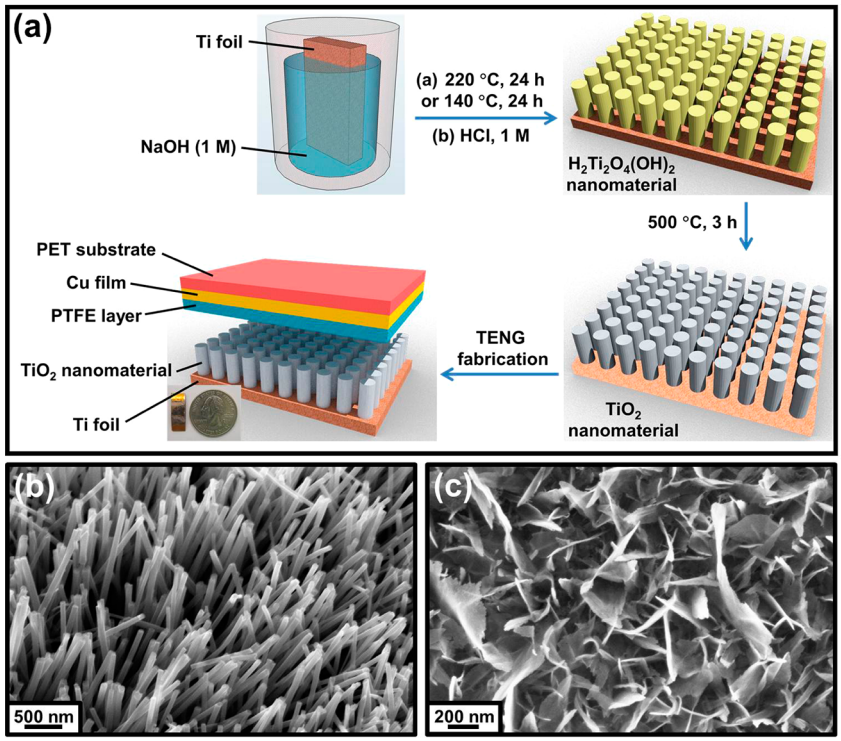

Figure 1. (a) Fabrication process of the TENG. (b and c) SEM images of the Ti foil covered with TNW array (b) and TNS array (c).

In this paper, we prove not only that the TENG can be used as a sensor for catechin detection, but also that the chemical modification is effective to enhance the electrical output of TENG if it is used as a power source. TiO_2 nanomaterial arrays are designed as contact materials in order to selectively capture catechin and enlarge the contact area of TENG. On the basis of this unique structure, the output voltage and current density of the as-developed TENG can be enhanced from 4.3 to 21.3 V and 1.1 to 3.2 $\mu A/cm^2$, respectively, when detecting catechin concentration over 0.5 mM. Under optimum conditions, this TENG is selective for catechin detection, with a detection limit of 5 μM and a linear range from 10 μM to 0.5 mM.

RESULTS AND DISCUSSION

The TENG has a layered structure based on two plates as schematically shown in Figure 1a. On the lower side, a layer of TiO_2 nanomaterial array is prepared as one of the contact materials. TiO_2 nanowire (TNW) array and TiO_2 nanosheet (TNS) array grown on Ti foil were prepared *via* a two-step synthesis process.[18] First, $H_2Ti_2O_4(OH)_2$ nanowire array and $H_2Ti_2O_4(OH)_2$ nanosheet array (Figure S1) were synthesized on Ti foil through a hydrothermal route in alkali solution combined with an ion-exchange process (acid treatment). Higher temperatures cause a faster reaction between Ti foil and NaOH, and hence, formed a denser $Na_2Ti_2O_4(OH)_2$ nanowire array. Then TNW array and TNS array can be obtained *via* heat treatment of the as-prepared $H_2Ti_2O_4(OH)_2$ nanowire array and $H_2Ti_2O_4(OH)_2$ nanosheet array. The mean diameters of TNW and TNS determined from scanning electron microscopy (SEM) images are 67.2 nm (Figure 1b) and 9.4 nm (Figure 1c), respectively. As the cross-sectional SEM images (Figure S2) show, the oriented nanowire array and nanosheet array are perpendicularly grown on the Ti foil, and the respective thicknesses of these films are 4.2 and 0.8 μm. Figure S3 illustrates X-ray diffraction (XRD) patterns of the as-prepared TNW array and TNS array. The characteristic facets of (101) and (200) are assigned for the anatase crystal phase (JCPDS No. 65-2900), and other peaks correspond to the Ti foil, revealing that their structures are mainly anatase phase. On the other plate, polyethylene terephthalate (PET) was selected as the material for substrate due to its flexibility, light weight, and low cost. A Cu thin film is laminated between the PET substrate and a layer of polytetrafluoroethylene (PTFE). PTFE has the advantages of flat surface and easy processing. According to the triboelectric series (Figure S4),[19] PTFE is triboelectric negative and has a large difference in ability to attract and retain electrons as compared to TiO_2, which will contribute a large electrical output of TENG.

Figure 2 illustrates the electricity generation process of TENG. PET substrate is omitted from the figure for the purpose of simplification. At the original position (Figure 2a), no charge transfers occur because these two plates are not in contact. Upon pressing the PTFE plate to contact with TiO_2 plate, electrons will transfer from the material at the more positive position in the triboelectric series to the one at the relatively negative

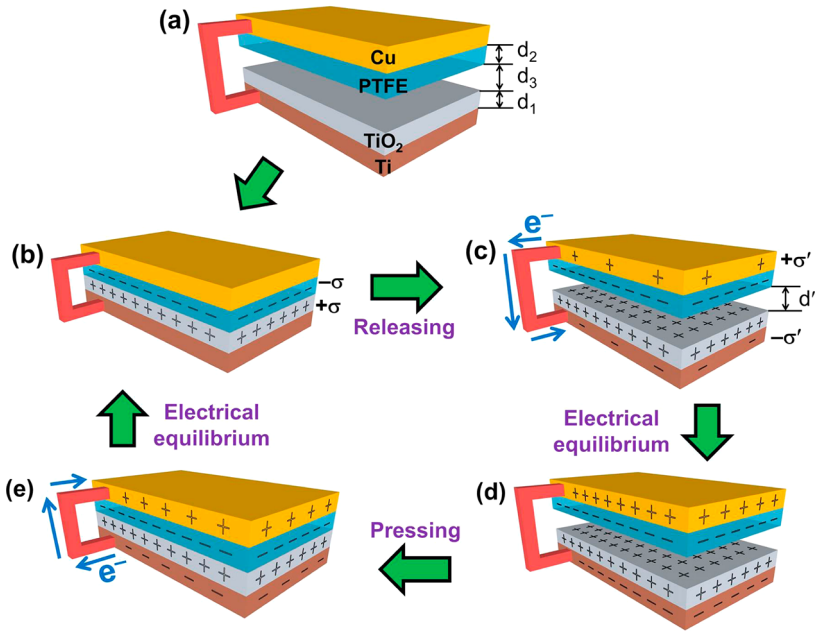

Figure 2. (a) Original position without mechanical force applied. (b) External force brings the two plates into contact, resulting in surface triboelectric charges. (c) Withdrawal of the force causes a separation and electrons flow from Cu electrode through external load to the Ti electrode. (d) Charge distribution of TENG after the electrical equilibrium. (e) External force applied again to make the two electrodes contact and induce the electrons flow from Ti electrode through external load to the Cu electrode.

position.[20] Hence, electrons will inject from TiO_2 to PTFE and result in positive charges on the TiO_2 surface and negative charges on the PTFE surface (Figure 2b). Once the force is withdrawn, a separation forms, and an electric potential difference is then established between these two plates. Such a potential difference drives electron flow through external loads from the Cu electrode to the Ti electrode to screen the positive triboelectric charges on the TiO_2 plate (Figure 2c). If we define electric potential of the bottom plate (U_{bottom}) as zero, electric potential of the top plate (U_{top}) can be expressed by

$$U_{top} = \frac{\sigma d'}{\varepsilon_0} \quad (1)$$

where σ is the triboelectric charge density, ε_0 is the vacuum permittivity, and d' is the gap distance between two plates at a given state. Therefore, the open-circuit voltage (V_{oc}) will keep increasing until reaching the maximum value when the PET plate fully reverts to the original position. By regarding the TENG as a flat-panel capacitor, the inducted charge density (σ') on the Cu electrode and the Ti electrode can be calculated as

$$\sigma' = \frac{\sigma d' \varepsilon_{rt} \varepsilon_{rp}}{d_1 \varepsilon_{rp} + d' \varepsilon_{rt} \varepsilon_{rp} + d_2 \varepsilon_{rt}} \quad (2)$$

where ε_{rt}, and ε_{rp} are the relative permittivity of TiO_2 and PTFE, respectively, and d_1 and d_2 are the thickness of the TiO_2 film and the PTFE layer, respectively. Because d_1, d_2, ε_{rt}, and ε_{rp} are constants, and the triboelectric charge density is stable for a relatively long time,[21] σ' is determined by the gap distance d'. Changing the d' will cause different charge distribution, finally achieving a new equilibrium (Figure 2d). The maximum value of σ' is obtained by substituting the d_3 for d' in the above equation. The gap distance d_3 of the as-developed TENG is designed as 0.3 cm. When the external force applied again to make the two electrodes contact, the electric potential difference starts diminishing as the two plates get closer to each other. As a result, the V_{oc} drops from the maximum value to zero when a full contact is made again between the plates. A reduction of the d' would make the PTFE plate a higher electric potential than the TiO_2 plate. As a consequence, electrons will flow from Ti electrode through external load to Cu electrode to screen the positive triboelectric charges on the PTFE plate (Figure 2e). This process corresponds to an instantaneous negative current.

Next, we used a mechanical shaker as the external force to impact the TENG. The TENG performance was determined by the V_{oc} and short-circuit current density (J_{sc}). Figure 3a indicates the V_{oc} of 4.3 V is switched between zero and a plateau value, which correspond to the contact and original position. We also measured the electrical output of the TENG with a reverse connection to the electrometer. The V_{oc} (Figure 3b) showed the opposite values in Figures 3a, proving that the measured signals were generated by the TENG. The J_{sc} reaches a value of 1.1 $\mu A/cm^2$ and exhibits AC behavior, with an equal amount of electrons flowing in opposite directions within one cycle (Figure 3c).

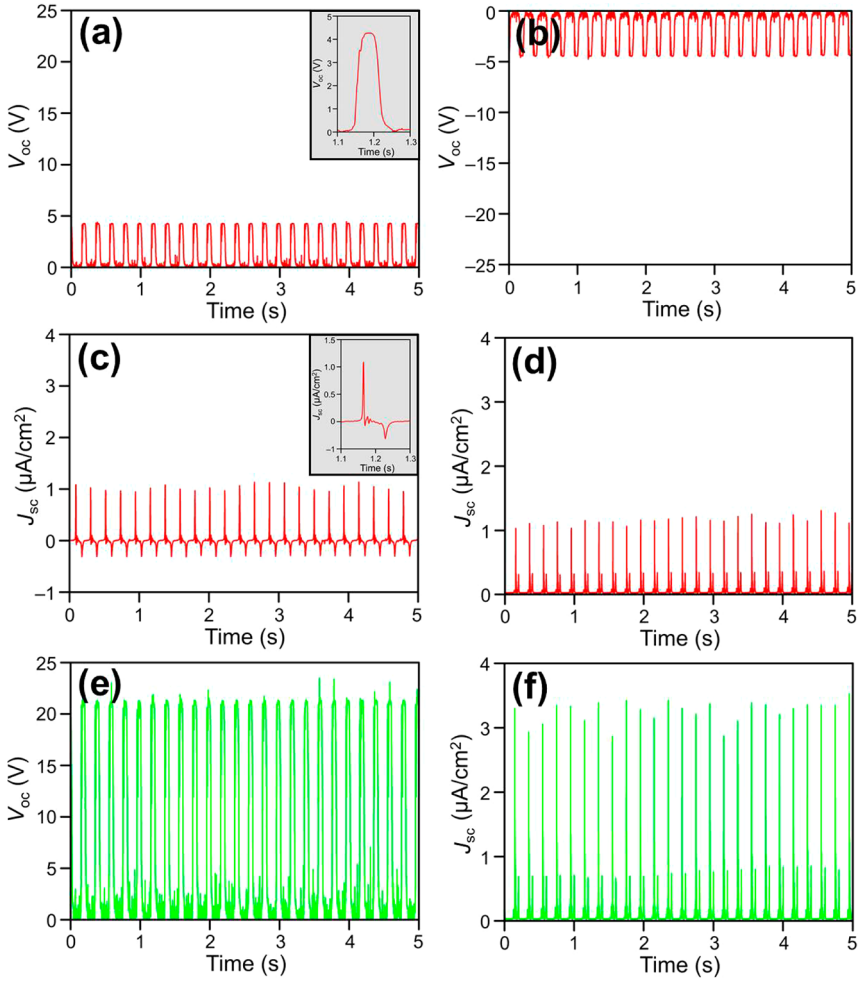

Figure 3. (a and b) The generated V_{oc} of the TNW array-based TENG at forward connection (a) and reversed connection (b) to the measurement system. (c and d) The generated J_{sc} of the TNW array-based TENG at forward connection (c) and after rectification by a full-wave bridge (d). Insets of (a) and (c): enlarged view of one cycle. (e and f) The generated V_{oc} (e) and rectified J_{sc} (f) of the TNW array-based TENG after reacting with 0.5-mM catechin solution.

The experimental data validate the working mechanism described in Figure 2. Furthermore, the AC output could be transformed to pulse output in the same direction simply by a full-wave rectifying bridge (Figure 3d). We then demonstrated the as-developed TENG can be utilized as a self-powered nanosensor for catechin detection. Phosphate solution (20 mM, pH 7.0) was used as the buffer and the reaction time was optimized to be 20 min. After the reaction, the TiO_2 plate was washed with water and dried at ambient temperature prior to the electrical measurement. Figure 3e,f exhibits the generated V_{oc} and J_{sc} of TNW array-based TENG after reacting in 0.5-mM catechin solution for 20 min and then dried. The generated V_{oc} is increased to 21.3 V (5.0 times) while the generated J_{sc} density is increased to 3.2 μA/cm^2 (2.9 times). This is the first demonstration of enhancing TENG's output by chemical modification.

We further compared the electrical output of TNW array-based TENG and TNS array-based TENG when detecting catechin solutions with different concentrations. Figure 4a,b manifests that the open-circuit voltage ratio $((V_{oc} - V_{oc}^{o})/V_{oc}^{o})$ of TNW array-based TENG and TNS array-based TENG both increased upon adding the catechin concentration. The linear relationships between the open-circuit voltage ratio and the catechin concentrations ranging from 10 μM to 0.5 mM (R^2 = 0.98) for TNW array-based TENG and 10 μM to 0.25 mM (R^2 = 0.97) for TNS array-based TENG. The relationships between the short-circuit current density ratio $((J_{sc} - J_{sc}^{o})/J_{sc}^{o})$ and catechin concentration (Figure S5) are similar to those in Figure 4a,b. The different linear ranges of TNW array-based TENG and TNS array-based TENG toward catechin detection is probably attributed to the different surface areas of TNW array and TNS array. TiO_2 nanomaterial array with larger surface area can adsorb more catechin molecules, which consequently contribute to the detection of catechin solution at higher concentration. The typical isotherms for nitrogen adsorption and desorption of the TNW array and TNS array are displayed in Figure 4c, which categorize them as type IV according to IUPAC classification.[22]

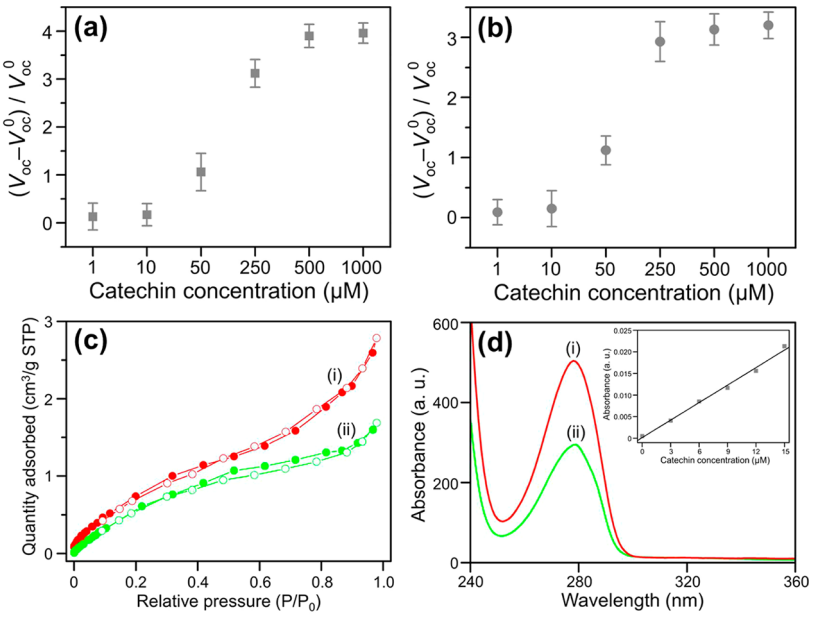

Figure 4. (a and b) The generated open-circuit voltage ratio ($(V_{oc} - V_{oc}^o)/V_{oc}^o$) of TNW array-based TENG (a) and TNS array-based TENG (b) when sensing catechin solutions with different concentrations. (c) N_2 adsorption and desorption isotherms of (i) TNW array and (ii) TNS array. Solid circles: adsorption; hollow circles: desorption. (d) Absorption spectra of the supernatants of catechin solutions containing (i) TNW array and (ii) TNS array. Inset of (d): the calibration curve of catechin concentration from absorption spectra.

The determined BET specific surface areas of TNW array and TNS array are 3.3 and 2.5 m^2/g, respectively, showing that the TNW array has a larger surface area than that of TNS array. We also measured the saturated adsorption concentration of catechin on TNW array and TNS array (Figure 2c). TNW array and TNS array were immersed in 10 μM solutions of catechin for 1 h. The absorption spectra of the related supernatants show the saturated adsorption concentrations of catechin on TNW array and TNS array are 6 and 3 μM, respectively. From these results, we can conclude that the TNW array has a larger surface area than that of TNS array, and hence contributes to the broader linear range toward catechin detection.

The main reason that causes the electrical output enhancement of TENG is the new hybrid property of TiO_2/catechin complex, which is arising from the ligand-to-metal charge transfer interaction between the enediol group of catechin and surface Ti atoms of TiO_2 nanomaterial.[23] Adding catechin solution to TNW induced an immediate change in the absorption spectrum and powder color (Figure 5a), indicating the formation of charge-transfer complex.[24] For bare TNW, the wavelength of the onset of absorption is located at 450 nm, while binding the catechin onto the surface of TNW shifts the onset of absorption to a longer wavelength (530 nm). To further investigate the charge-transfer mechanism, cyclic voltammetry (CV) technique was used to characterize the trap states in TNW array.[25] The trap states distributed within the band gap and partially occupied by nonequilibrium electrons[26] (electrons that are not in their lowest energy state) are the critical roles in the contact electrification process of semiconductor and insulating materials.[27,28] In Figure 5b, the CV curves of bare and catechin-modified

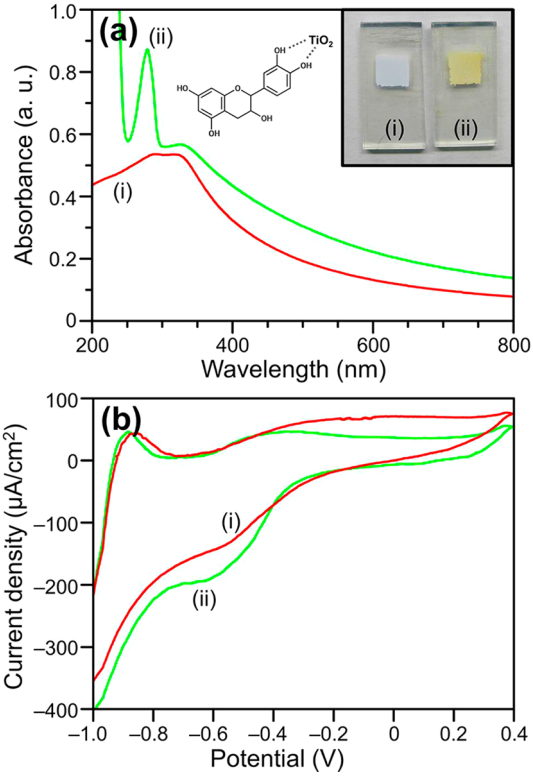

Figure 5. (a) Absorption spectra of TNW (i) before and (ii) after the catechin modification. (b) Cyclic voltammograms (scan rate: 50 mV s^{-1}) of TNW array (i) before and (ii) after the catechin modification in N_2-saturated 20-mM phosphate buffer.

TNW array in the range of −1.0 to 0.4 V are measured. The conduction band edge of TiO_2 at pH 6.8 is approximately at −0.67 V *vs* Ag/AgCl reference electrode.[29] A feature at −0.54 V in bare TNW array corresponds to the filling states below the conduction band edge, confirming the presence of trap states.[30,31] After the binding of catechin onto TNW array, the peak reaches a potential of −0.62 V close to the flat band potential (−0.67 V), and shows more electrons are filled in the trap states. The increase of electron population in the trap states of TNW array indicates that more charges will transfer from TiO_2 plate to PTFE plate upon the TENG operation, resulting in the enhanced TENG performance.

CONCLUSION

In summary, we have developed the triboelectric effect-based nanosensor for catechin detection by utilizing TiO_2 nanomaterial array as the probe and contact material. This novel self-powered TENG is highly sensitive (detection limit of 5 μM and linear range of 10 μM to 0.5 mM) and selective for catechin detection, demonstrating great potential for the determination of catechin concentrations in real samples. Among the currently proposed TENG designs, this study is first of its kind to increase the TENG performance through chemical modification. With the charge transfer mechanism from catechin to TiO_2 nanomaterial, the generated V_{oc} is increased from 4.3 V up to 21.3 V (5.0 times) while the generated I_{sc} density is increased from 1.1 $\mu A/cm^2$ up to 3.2 $\mu A/cm^2$ (2.9 times). With such outstanding results, we believe that this unprecedentedly innovative mechanism will form the foundation for high-power TENG and contribute to the future development of self-powered nanosensors.

METHODS

Growth of TiO_2 Nanowire Array and TiO_2 Nanosheet Arrays on Ti Foils. Pieces of Ti foils (1.2 cm × 3.6 cm), ultrasonically cleaned in acetone, ethanol, and water for 10 min each, were placed in separate 25 mL Teflon-lined stainless steel autoclaves filled with NaOH aqueous solutions (1 M, 20 mL). The sealed autoclaves were heated in ovens at different temperatures of 140 °C ($Na_2Ti_2O_4(OH)_2$ nanosheet array) and 220 °C ($Na_2Ti_2O_4(OH)_2$ nanowire array) for 24 h, and then cooled in air. After the first-step hydrothermal reaction, Ti foils covered with $Na_2Ti_2O_4(OH)_2$ nanosheet array or $Na_2Ti_2O_4(OH)_2$ nanowire array were washed with water and immersed in HCl solutions (1 M, 20 mL) for 10 min to replace Na^+ with H^+, forming $H_2Ti_2O_4(OH)_2$ nanosheet array and $H_2Ti_2O_4(OH)_2$ nanowire array on Ti foils. After that, Ti foils were removed from HCl solution and washed with water again, then dried at ambient temperature. TiO_2 nanosheet array and TiO_2 nanowire array on Ti foils were obtained after a heat treatment of the samples in an oven at 500 °C for 3 h.

TENG Fabrication. A thin film of Cu (50 nm) was deposited on a purchased PTFE layer (25 μm) by e-beam evaporator. Then, the Cu/PTFE composite was glued to the inner surface of the bending PET substrate. This is the top (PTFE) plate. For catechin detection, phosphate solution (20 mM, pH 7.0) was used as the buffer. Fixed volumes (20 μL) of buffer solutions containing different catechin concentrations were dropped onto the TiO_2 plates. After 20 min, the reacted plates were washed with water and dried at ambient temperature. Finally, conducting wires were connected to the two Ti and Cu electrodes as leads for subsequent electrical measurements. The gap distance was designed to be 0.3 cm.

Characterization. A LEO 1550 field emission scanning electron microscope (SEM) was used to measure the size and shape of the $H_2Ti_2O_4(OH)_2$ and TiO_2 nanomaterials. A PANalytical X'Pert PRO diffractometer (Almelo, The Netherlands) with Cu Kα radiation (λ = 0.15418 nm) was used to measure X-ray diffraction (XRD) patterns of the as-prepared TiO_2 nanomaterials. A double beam UV−Vis spectrophotometer (JASCO V-630) was used to measure the absorption spectra of the catechin solutions and bare and catechin-modified TiO_2 nanowires. The electrical outputs of the as-developed TENGs were measured using a programmable electrometer (Keithley Model 6514) and a low-noise current preamplifier (Stanford Research System Model SR570).

Conflict of Interest: The authors declare no competing financial interest.

Supporting Information Available: SEM images of $H_2Ti_2O_4(OH)_2$ nanowire array and $H_2Ti_2O_4(OH)_2$ nanosheet array, cross-sectional SEM images of TNW array and TNS array, XRD patterns of TNW array and TNS array, a modified triboelectric series, the generated short-circuit current density ratio of TNW array-based TENG and TNS array-based TENG when sensing catechin solutions with different concentrations, and SEM images of TNW array and TNS array after the TENG was operating for 3 h. This material is available free of charge *via* the Internet at http://pubs.acs.org.

Acknowledgment. This work was supported by Airforce, MURI, U.S. Department of Energy, Office of Basic Energy Sciences (DE-FG02-07ER46394), NSF, Taiwan (NSC 101-2917-I-564-029), and the Knowledge Innovation Program of the Chinese Academy of Sciences (KJCX2-YW-M13). The technology reported here is protected by patents.

REFERENCES AND NOTES

1. Qin, Y.; Wang, X. D.; Wang, Z. L. Microfibre−Nanowire Hybrid Structure for Energy Scavenging. *Nature* **2008**, *451*, 809–813.
2. Lee1, M.; Chen, C.-Y.; Wang, S.; Cha, S. N.; Park, Y. J.; Kim, J. M.; Chou, L.-J.; Wang, Z. L. A Hybrid Piezoelectric Structure for Wearable Nanogenerators. *Adv. Mater.* **2013**, *24*, 1759–1764.
3. Yang, Y.; Guo, W.; Pradel, K. C.; Zhu, G.; Zhou, Y.; Zhang, Y.; Hu, Y.; Lin, L.; Wang, Z. L. Pyroelectric Nanogenerators for Harvesting Thermoelectric Energy. *Nano Lett.* **2012**, *12*, 2833–2838.
4. Snyder, G. J.; Toberer, E. S. Complex Thermoelectric Materials. *Nat. Mater.* **2008**, *7*, 105–114.
5. Tian, B.; Zheng, X.; Kempa, T. J.; Fang, Y.; Yu, N.; Yu, G.; Huang, J.; Lieber, C. M. Coaxial Silicon Nanowires as Solar Cells and Nanoelectronic Power Sources. *Nature* **2007**, *449*, 885–890.
6. O'Regan, B.; Grätzel, M. A Low-Cost, High-Efficiency Solar Cell Based on Dye-Sensitized Colloidal TiO_2 Films. *Nature* **2001**, *353*, 737–740.
7. Wang, Z. L.; Zhu, G.; Yang, Y.; Wang, S.; Pan, C. Progress in Nanogenerators for Portable Electronics. *Mater. Today* **2012**, *15*, 532–543.
8. Wang, Z. L.; Wu, W. Nanotechnology-Enabled Energy Harvesting for Self-Powered Micro-/Nanosystems. *Angew. Chem., Int. Ed.* **2012**, *47*, 11700–11721.
9. Fan, F.-R.; Tian, Z.-Q.; Wang, Z. L. Flexible Triboelectric Generator. *Nano Energy* **2012**, *1*, 328–334.
10. Fan, F.-R.; Lin, L.; Zhu, G.; Wu, W.; Zhang, R.; Wang, Z. L. Transparent Triboelectric Nanogenerators and Self-Powered Pressure Sensors Based on Micropatterned Plastic Films. *Nano Lett.* **2012**, *12*, 3109–3114.

11. Zhu, G.; Pan, C.; Guo, W.; Chen, C.-Y.; Zhou, Y.; Yu, R.; Wang, Z. L. Triboelectric-Generator-Driven Pulse Electrodeposition for Micropatterning. *Nano Lett.* **2012**, *12*, 4960–4965.
12. Zhong, J.; Zhong, Q.; Fan, F.; Zhang, Y.; Wang, S.; Hu, B.; Wang, Z. L.; Zhou, J. Finger Typing Driven Triboelectric Nanogenerator and its Use for Instantaneously Lighting up LEDs *Nano Energy* **2013**, in press (dx.doi.org/10.1016/j.nanoen.2012.11.015).
13. Wang, S.; Lin, L.; Wang, Z. L. Nanoscale Triboelectric-Effect-Enabled Energy Conversion for Sustainably Powering Portable Electronics. *Nano Lett.* **2012**, *12*, 6339–6346.
14. Diaz, A. F.; Felix-Navarro, R. M. A Semi-Quantitative Tribo-Electric Series for Polymeric Materials: The Influence of Chemical Structure and Properties. *J. Electrost.* **2004**, *62*, 277–290.
15. Zhang, X.-S.; Han, M.-D.; Wang, R.-X.; Zhu, F.-Y.; Li, Z.-H.; Wang, W.; Zhang, H.-X. Frequency-Multiplication High-Output Triboelectric Nanogenerator for Sustainably Powering Biomedical Microsystems. *Nano Lett.* **2013**, *13*, 1168–1172.
16. Zhu, G.; Lin, Z.-H.; Jing, Q.; Bai, P.; Pan, C.; Yang, Y.; Zhou, Y.; Wang, Z. L. Toward Large-Scale Energy Harvesting by a Nanoparticle-Enhanced Triboelectric Nanogenerator. *Nano Lett.* **2013**, *13*, 847–853.
17. Lin, Z.-H.; Zhu, G.; Zhou, Y. S.; Yang, Y.; Bai, P.; Chen, J.; Wang, Z. L. Self-Powered Triboelectric Nanosensor for Mercury Ion Detection. *Angew. Chem., Int. Ed.* **2013**, DOI: 10.1002/anie.201300437.
18. Liao, J.-Y.; Lei, B.-X.; Chen, H.-Y.; Kuang, D.-B.; Su, C.-Y. Oriented Hierarchical Single Crystalline Anatase TiO_2 Nanowire Arrays on Ti-Foil Substrate for Efficient Flexible Dye-Sensitized Solar Cells. *Energy Environ. Sci.* **2012**, *5*, 5750–5757.
19. McCarty, L. S.; Whitesides, G. M. Electrostatic Charging Due to Separation of Ions at Interfaces: Contact Electrification of Ionic Electrets. *Angew. Chem., Int. Ed.* **2008**, *47*, 2188–2207.
20. Lacks, D. J.; Sankaran, R. M. Contact Electrification of Insulating Materials. *J. Phys. D: Appl. Phys.* **2011**, *44*, 453001.
21. Watson, P. K.; Yu, Z. Z. The Contact Electrification of Polymers and the Depth of Charge Penetration. *J. Electrost.* **1997**, *40*−*41*, 67–72.
22. Chen, J. S.; Tan, Y. L.; Li, C. M.; Cheah, Y. L.; Luan, D.; Madhavi, S.; Boey, F. Y. C.; Archer, L. A.; Lou, X. W. Constructing Hierarchical Spheres from Large Ultrathin Anatase TiO_2 Nanosheets with Nearly 100% Exposed (001) Facets for Fast Reversible Lithium Storage. *J. Am. Chem. Soc.* **2010**, *132*, 6124–6130.
23. Rajh, T.; Chen, L. X.; Lukas, K.; Liu, T.; Thurnauer, M. C.; Tiede, D. M. Surface Restructuring of Nanoparticles: An Efficient Route for Ligand-Metal Oxide Crosstalk. *J. Phys. Chem. B* **2002**, *106*, 10543–10552.
24. Lee, K. H.; Chiang, C. K.; Lin, Z. H.; Chang, H. T. Determining Enediol Eompounds in Tea Using Surface-Assisted Laser Desorption/Ionization Mass Spectrometry with Titanium Dioxide Nanoparticle Matrices. *Rapid Commun. Mass Spectrom.* **2007**, *21*, 2023–2030.
25. Garza, L. D. L.; Saponjic, Z. V.; Dimitrijevic, N. M.; Thurnauer, M. C.; Rajh, T. Surface States of Titanium Dioxide Nanoparticles Modified with Enediol Ligands. *J. Phys. Chem. B* **2006**, *110*, 680–686.
26. Lowell, J.; Truscott, W. S. Triboelectrification of Identical Insulators. II. Theory and Further Experiments. *J. Phys. D: Appl. Phys.* **1986**, *19*, 1281.
27. Hao, E.; Anderson, N. A.; Asbury, J. B.; Lian, T. Effect of Trap States on Interfacial Electron Transfer between Molecular Absorbates and Semiconductor Nanoparticles. *J. Phys. Chem. B* **2002**, *106*, 10191–10198.
28. Kron, A.; Reitberger, T.; Stenberg, B. Luminescence from γ- and β-Irradiated HDPE and LLDPE. *Polym. Int.* **1997**, *42*, 131–137.
29. Dimitrijevic, N. D.; Saponjic, Z. V.; Bartels, D. M.; Thurnauer, M. C.; Tiede, D. M.; Rajh, T. Revealing the Nature of Trapping Sites in Nanocrystalline Titanium Dioxide by Selective Surface Modification. *J. Phys. Chem. B* **2003**, *107*, 7368–7375.
30. Kavan, L.; Grätzel, M.; Rathousky, J.; Zukal, A. Nanocrystalline TiO_2 (Anatase) Electrodes: Surface Morphology, Adsorption, and Electrochemical Properties. *J. Electrochem. Soc.* **1996**, *143*, 394–400.
31. Boschloo, G.; Fitzmaurice, D. Spectroelectrochemical Investigation of Surface States in Nanostructured TiO_2 Electrodes. *J. Phys. Chem. B* **1999**, *103*, 2228–2231.